Electronic Supplementary Material (ESI) for Journal of Materials Chemistry A.

Supporting Information

Metallic La_3C_2 monolayer with remarkable activity for hydrogen evolution reaction: a first-principles study

Huan Lou[1,2], and Guochun Yang[1*]

1. State Key Laboratory of Metastable Materials Science & Technology and Key Laboratory for Microstructural Material Physics of Hebei Province, School of Science, Yanshan University, Qinhuangdao 066004, China

2. Department of Applied Physics, School of Science, Jiangsu University of Science and Technology, Zhenjiang 212100, China

Corresponding Author
*E-mail:yanggc468@nenu.edu.cn; yanggc@ysu.edu.cn

Index **Page**

Computational Details

The particle swarm optimization (PSO) method within the evolutionary algorithm implemented in the Crystal structure AnaLYsis by Particle Swarm Optimization (CALYPSO) code[1,2] was employed to find the lowest energy structures of the La_xC_y (x = 1-4, y = 1-4) monolayers. Unit cells containing 1, 2, and 4 formula units (f.u.) were considered. In the first step, random structures with certain symmetry are constructed in which atomic coordinates are generated by the crystallographic symmetry operations. Local optimizations using the VASP code[3] were done with the conjugate gradients method and stopped when Gibbs free energy changes became smaller than 1×10^{-5} eV per cell. After processing the first-generation structures, 60% of them with lower Gibbs free energies are selected to construct the next generation structures by Particle Swarm Optimization (PSO). 40% of the structures in the new generation are randomly generated. A structure fingerprinting technique of bond characterization matrix is applied to the generated structures, so that identical structures are strictly for bidden. These procedures significantly enhance the diversity of the structures, which is crucial for structural global search efficiency. In most cases, structural searching simulations for each calculation were stopped after generating 1000 ~ 1200 structures (*e.g.* about 20-30 generations).

The local structural relaxations and electronic properties calculations were performed in the framework of the density functional theory (DFT)[4] within the generalized gradient approximation (GGA)[5] as implemented in the VASP code. The cutoff energy of the plane-wave expansions is set to 500 eV. First-principles molecular dynamics (MD)[6] simulations for a large supercell were performed at different temperatures of 500 K. The supercells adopt 5 × 5 × 1 for La_2C with P-3m1 symmetry, 5 × 5 × 1 for La_3C_2 with P-3m1 symmetry, 3 × 3 × 1 for La_2C_3 with C2/m symmetry, and 3 × 4 × 1 for LaC_2 with *Pmmn* symmetry. MD simulation in NVT ensemble lasted for 10 ps with a time step of 1.0 fs. The temperature was controlled by using the Nosé-Hoover method.

Cohesive energy

Cohesive energy is widely used to ascertain the feasibility for experimental synthesis of the predicted 2D materials. Here, the cohesive energy E_{coh} is calculated based on the equation of

$E_{coh} = (x \times E_{La} + y \times E_C - E_{La_xC_y})/(x + y)$, where E_{La}, E_C, and $E_{La_xC_y}$ are the energies of La, C atom and 2D La_xC_y unit cell, respectively.

Supporting Figures

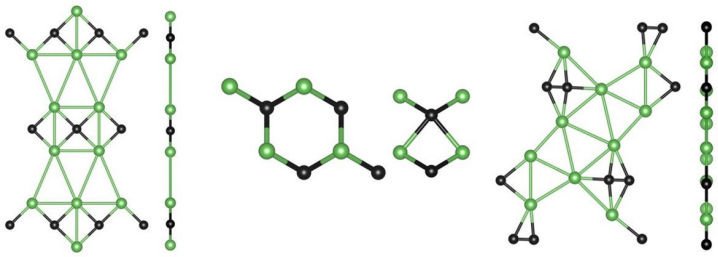

Figure S1. Top and side view of some other lower-energy structures of La_2C stoichiometric ratio along with structural symmetry and relative energy with respect to the *P*-3*m*1 La_2C monolayer.

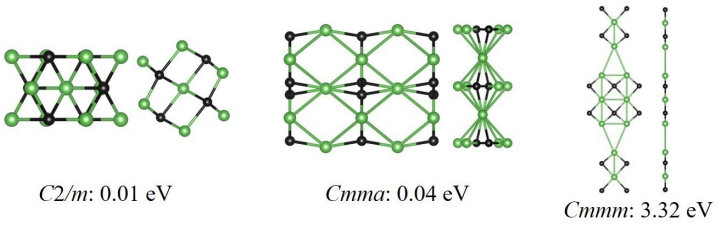

Figure S2. Top and side view of some other lower-energy structures of La_3C_2 stoichiometric ratio along with structural symmetry and relative energy with respect to the *P*-3*m*1 La_3C_2 monolayer.

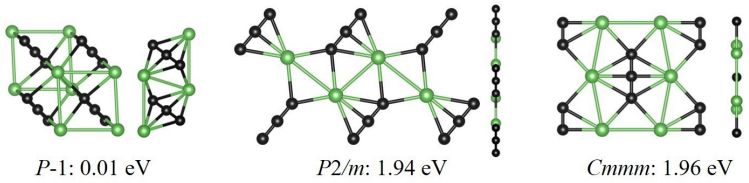

Figure S3. Top and side view of some other lower-energy structures of La_2C_3 stoichiometric ratio along with structural symmetry and relative energy with respect to the *C*2/*m* La_2C_3 monolayer.

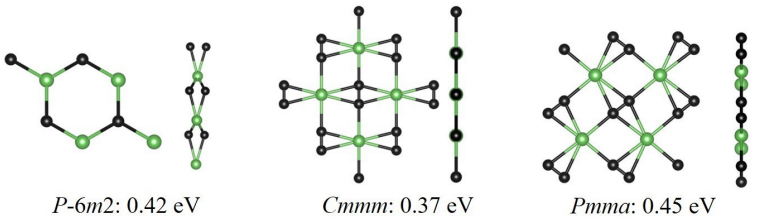

Figure S4. Top and side view of some other lower-energy structures of La_2C stoichiometric ratio along with structural symmetry and relative energy with respect to the *Pmmn* La_2C monolayer.

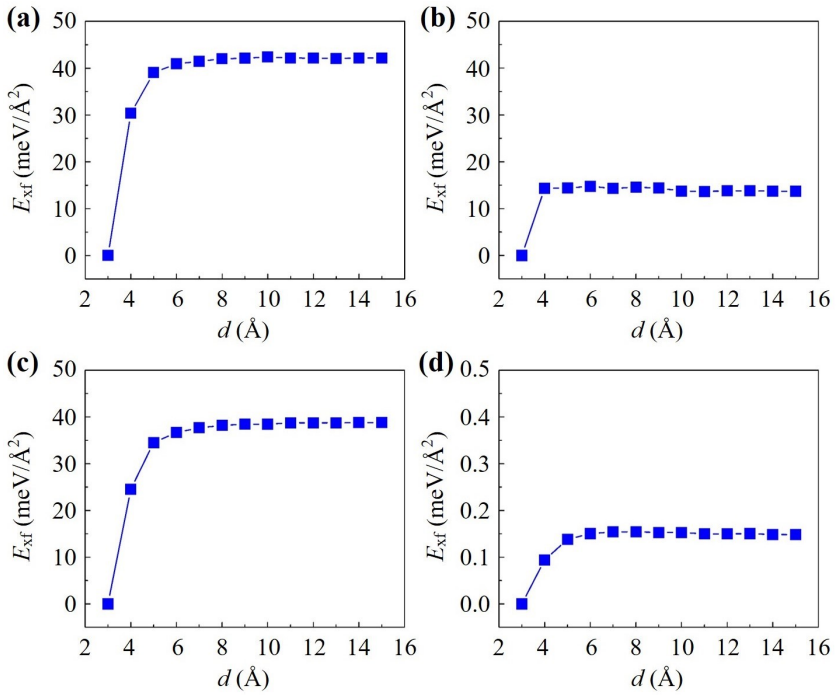

Figure S5. Calculated exfoliation energy vs separation distance *d* for the La_xC_y monolayer deposited on the graphite surface with five atomic thickness, where *d* indicates the interlayer distance between La_xC_y and graphite.

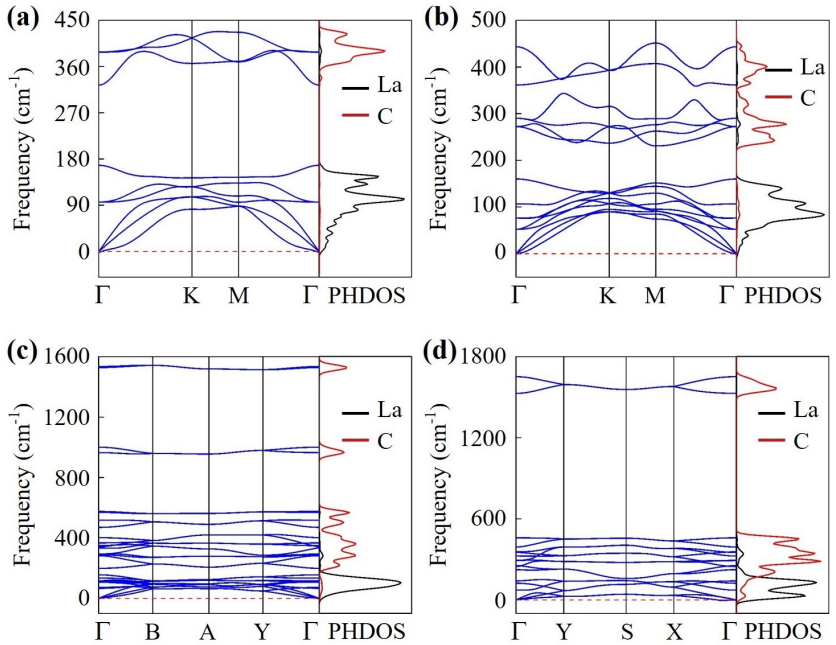

Figure S6. Phonon dispersive curves of the (a) La_2C, (b) La_3C_2, (c) La_2C_3, and (d) LaC_2 monolayers. The phonon maximum frequencies of four monolayers are 428, 451, 1542, and 1651 cm^{-1}, respectively.

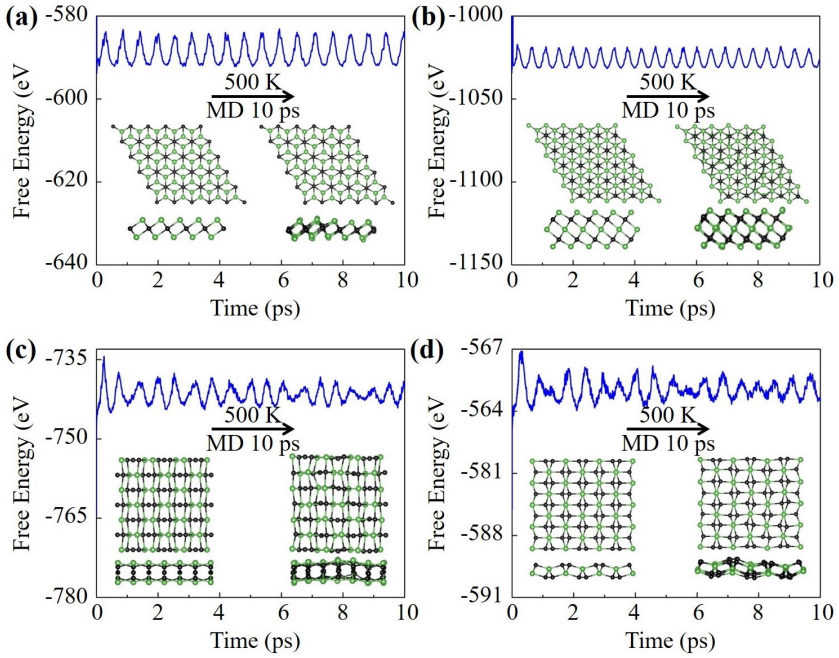

Figure S7. Snapshots of the final frame of the La_xC_y monolayers at time of 10 ps during AIMD simulations under the temperatures of 500 K, (a) La_2C, (b) La_3C_2, (c) La_2C_3, and (d) LaC_2 monolayers.

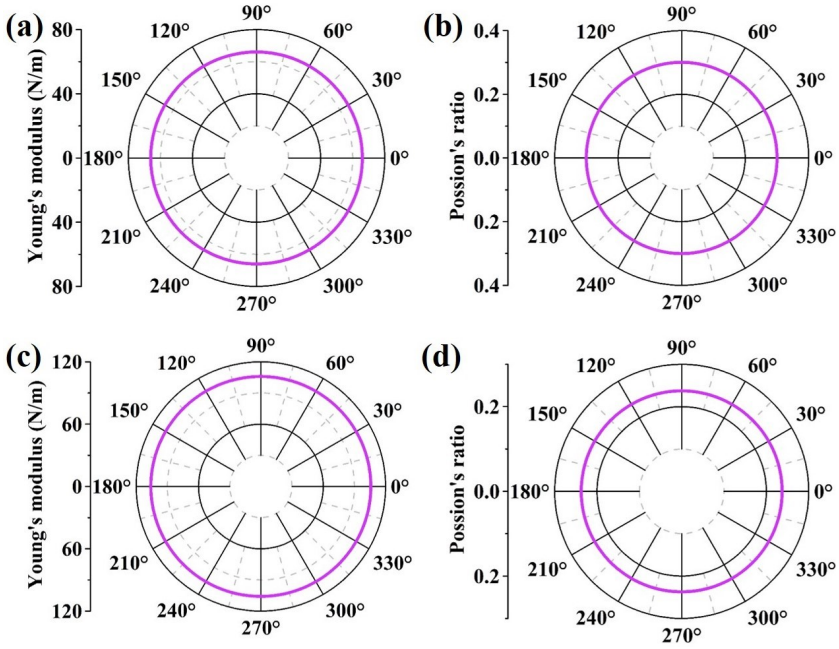

Figure S8. (Color online) Calculated orientation-dependent (a) Youngs's modulus $E(\theta)$, (b) Poisson's ratio $v(\theta)$ of the La_2C monolayer, (c) Youngs's modulus $E(\theta)$, and (d) Poisson's ratio $v(\theta)$ of the La_3C_2 monolayer.

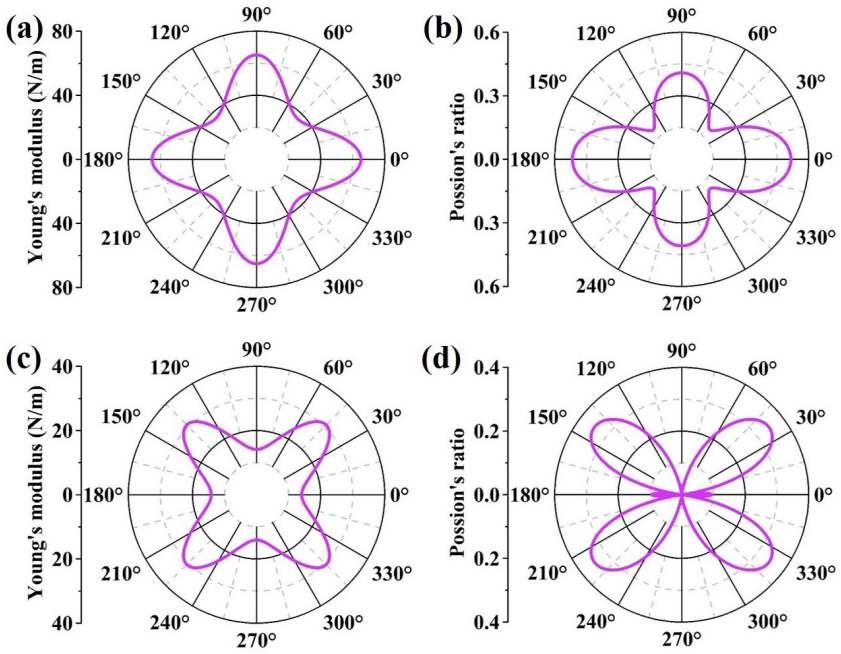

Figure S9. (Color online) Calculated orientation-dependent (a) Youngs's modulus $E(\theta)$, (b) Poisson's ratio $v(\theta)$ of the La_2C_3 monolayer, (c) Youngs's modulus $E(\theta)$, and (d) Poisson's ratio $v(\theta)$ of the LaC_2 monolayer.

Based on Born-Huang stability criteria, the mechanical stability of La_xC_y (x = 2-3, y = 2-3) monolayers are estimated by the strain-energy method.[7] The elastic constants of the La_2C monolayer are C_{11} = 188.67 N m^{-1}, C_{12} = 56.65 N m^{-1}, and C_{66} = 66.01 N m^{-1} (Figures S8a-b). For the La_3C_2 monolayer, the elastic constants are C_{11} = 277.47 N m^{-1}, C_{12} = 65.81 N m^{-1}, and C_{66} = 105.83 N m^{-1} (Figures S8c-d). Thus, the La_2C and La_3C_2 monolayers are satisfy the Born-Huang criteria of a mechanically stable 2D material (*e.g.* $C_{11} > 0$ and $C_{11} > |C_{12}|$). For the La_2C_3 monolayer, the elastic constants obtained are C_{11} = 150.45 N m^{-1}, C_{12} = 61.47 N m^{-1}, C_{22} = 119.15 N m^{-1}, and C_{66} = 65.13 N m^{-1} (Figures S9a-b). The obtained elastic constants of the LaC_2 monolayer are C_{11} = 125.57 N m^{-1}, C_{12} = -3.64 N m^{-1}, C_{22} = 38.52 N m^{-1}, and C_{66} = 14.10 N m^{-1} (Figures S9c-d). The La_2C_3 and LaC_2 monolayers satisfy the generalized elastic stability criteria as follows: $C_{11} > 0$, $C_{66} > 0$ and $C_{11} * C_{22} > C_{12} * C_{12}$. Therefore, the La_2C, La_3C_2, La_2C_3, and LaC_2 monolayers are mechanical stable.

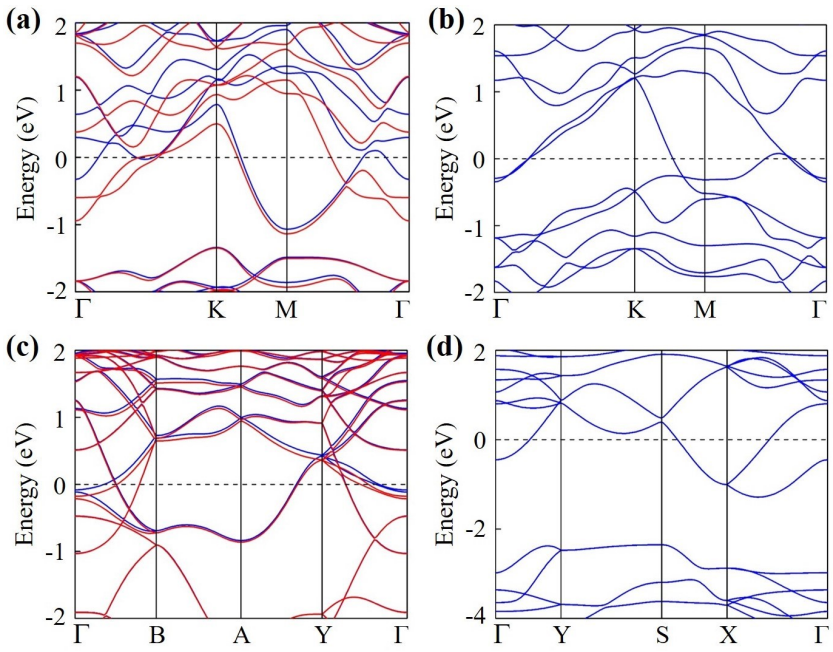

Figure S10. Band structures of the (a) La_2C, (b) La_3C_2, (c) La_2C_3, and (d) LaC_2 monolayers. The red and blue solid lines are spin-up bands and spin-down bands, respectively.

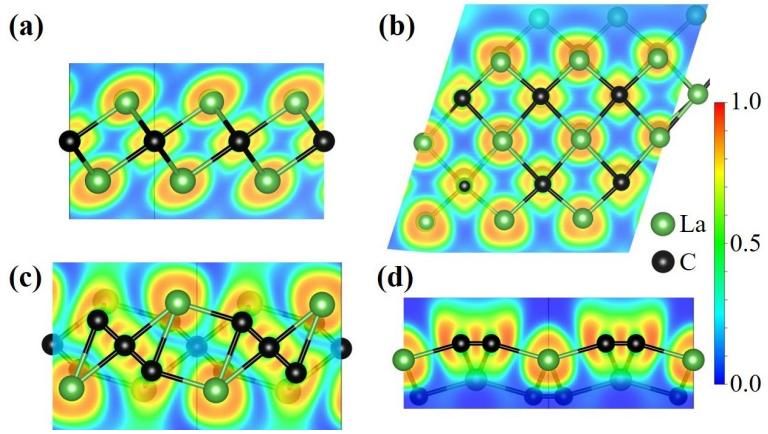

Figure S11. Electron localization function (ELF) map and crystal structures of the (a) La_2C, (b) La_3C_2, (c) La_2C_3, and (d) LaC_2 monolayers.

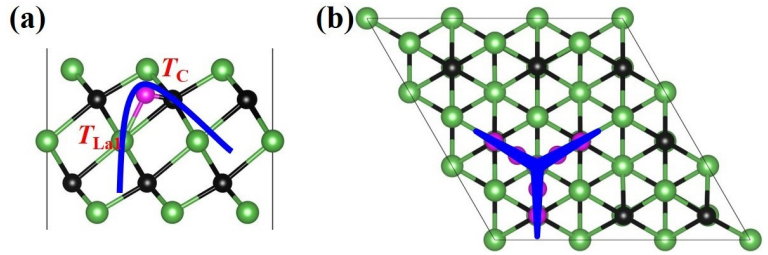

Figure S12. Schematic diagram of the optimized hydrogen atom at the active sites of the La_3C_2 monolayer. (a) Parabolic shape is formed through the hydrogen atom on each active site T_{La1}, B, and T_C, (b) These active sites make up the windmill shape of wind-powered generation centered on La_1 atom. The green, black, and pink balls represent La, C, and H atoms, respectively.

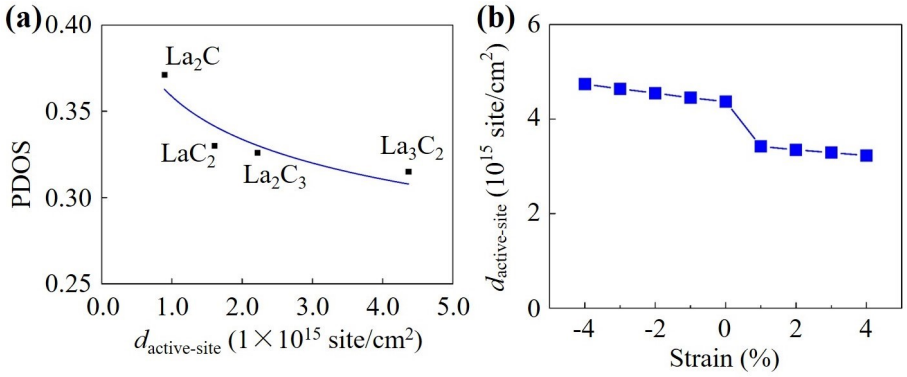

Figure S13. (a) The relationship between the sum of La p, d, and f of at Fermi level and the activity site density in the corresponding monolayer. (b) The relationship between active site density and biaxial strain of the La_3C_2 monolayer.

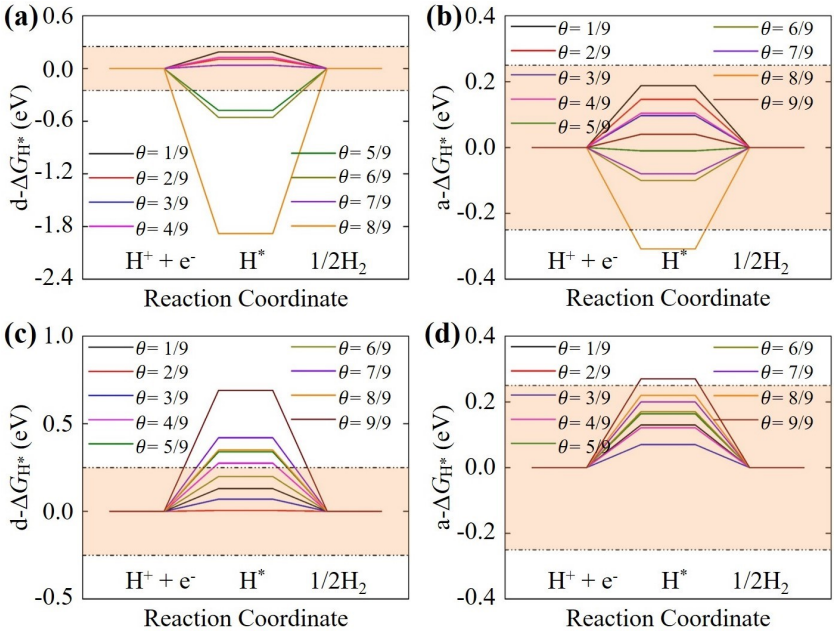

Figure S14. Calculated differential Gibbs free energies as a function of H coverage on the La-C monolayers. (a) d-ΔG_{H*} and (b) a-ΔG_{H*} of the La_2C monolayer, (c) d-ΔG_{H*} and (d) a-ΔG_{H*} of the (b) LaC_2 monolayer. The highlighted in orange denotes the free energy window of $\pm$0.25 eV.

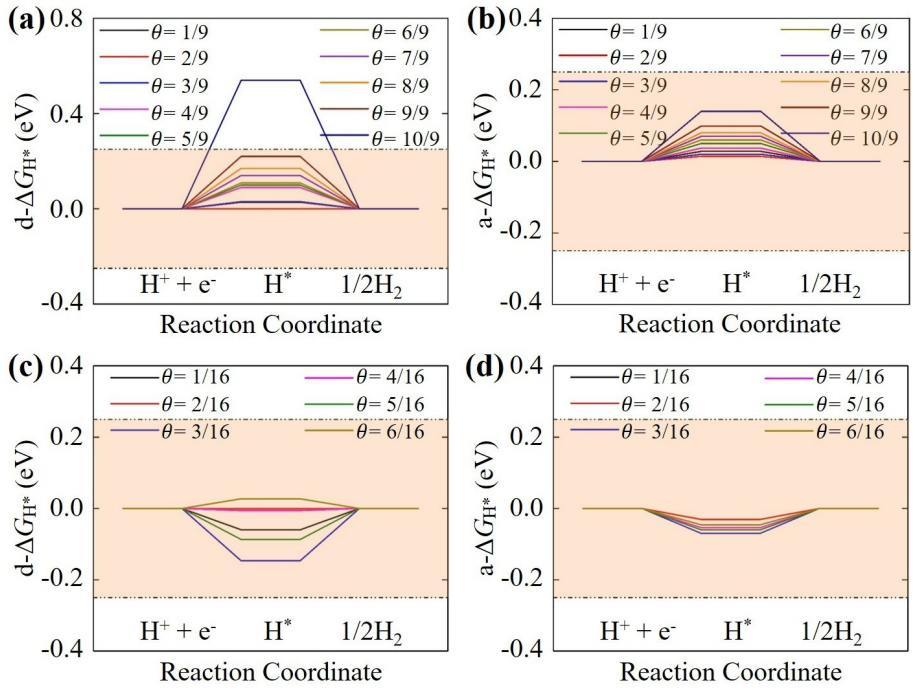

Figure S15. Calculated differential Gibbs free energies as a function of H coverage on the La-C monolayers. (a) d-$^{\Delta G_{H*}}$ and (b) a-$^{\Delta G_{H*}}$ for H adsorption on *B* site of the La_3C_2 monolayer, (c) d-$^{\Delta G_{H*}}$ and (d) a-$^{\Delta G_{H*}}$ for H adsorption on *H* site of the La_2C_3 monolayer.

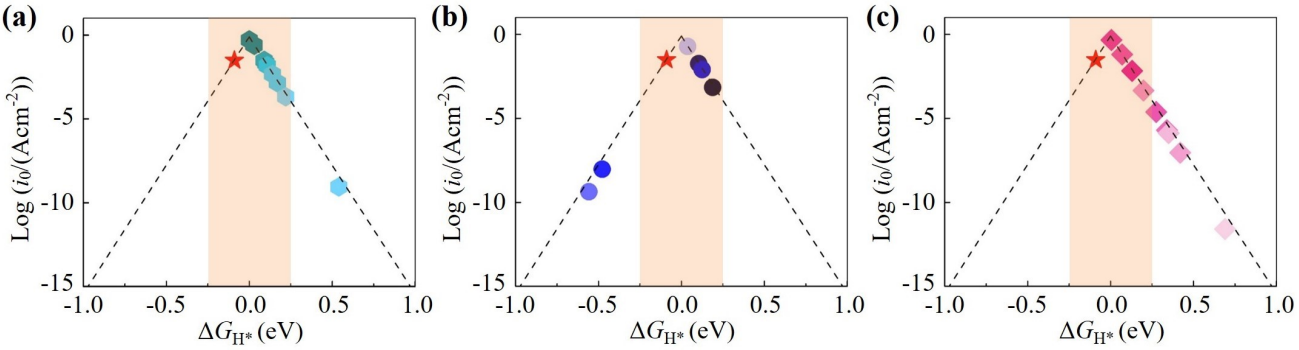

Figure S16. (a) Volcano curve of exchange current density i_0 as a function of d-$^{\Delta G_{H*}}$ with increasing H coverage, H adsorption on *B* site of the La_3C_2 monolayer, (b) La_2C monolayer, (c) LaC_2 monolayer. The color changes from light to dark with H coverage. The value of Pt is inserted by a red star for comparison.

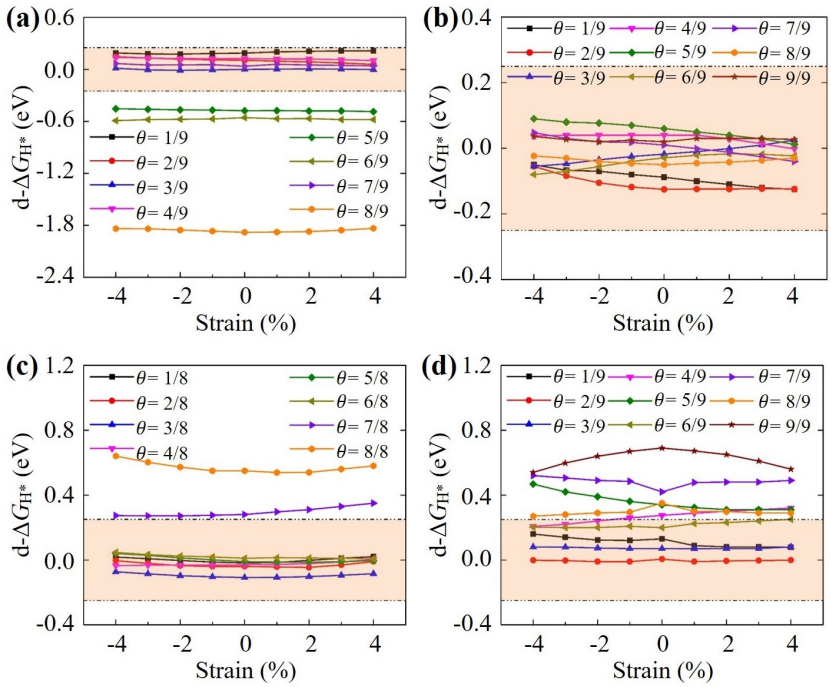

Figure S17. Variation of the free energies (d-ΔG_{H*}) of H adsorption as a function of the La_xC_y monolayers with strain, (a) La_2C, (b) La_3C_2, (c) La_2C_3, and (d) LaC_2 monolayers. The highlighted in orange denotes the free energy window of $\pm$ 0.25 eV.

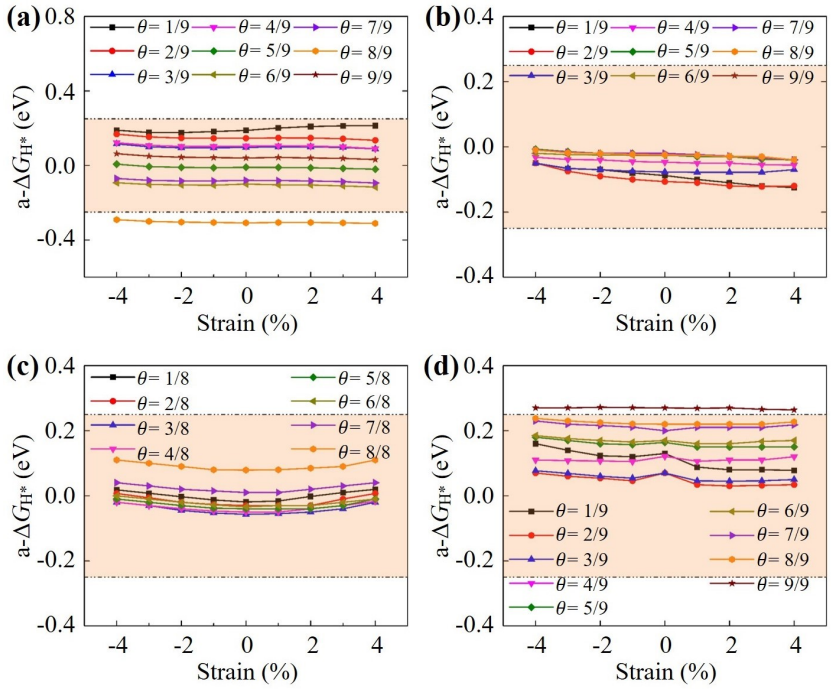

Figure S18. Variation of the free energies (a-ΔG_{H*}) of H adsorption as a function of the La_xC_y monolayers with strain, (a) La_2C, (b) La_3C_2, (c) La_2C_3, and (d) LaC_2 monolayers. The highlighted in

orange denotes the free energy window of $\pm$ 0.25 eV.

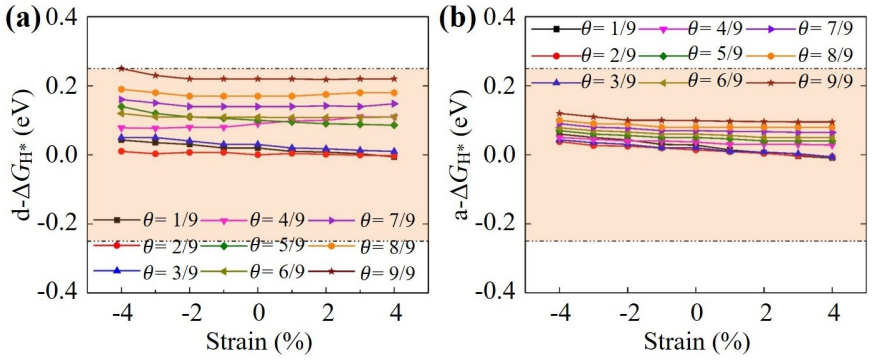

Figure S19. Calculated differential Gibbs free energies as a function of H coverage on *B* site the La_3C_2 monolayer with strain, (a) d-$^{\Delta G_{H*}}$ and (b) a-$^{\Delta G_{H*}}$. The highlighted in orange denotes the free energy window of $\pm$ 0.25 eV.

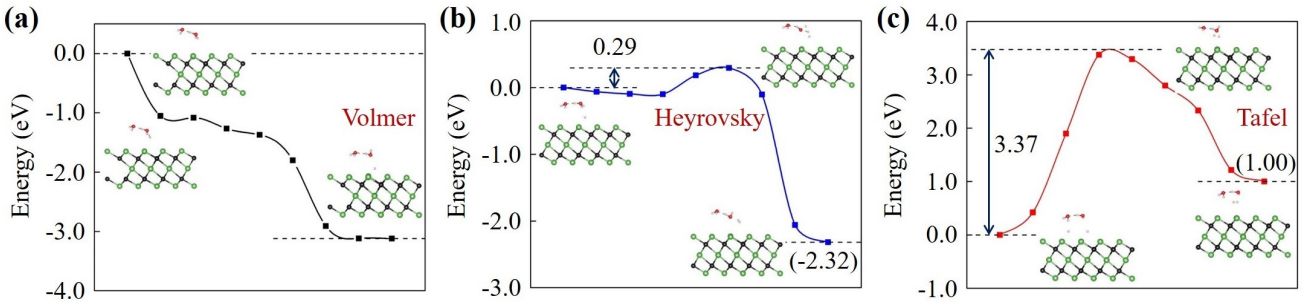

Figure S20. The HER reaction processes of the La_3C_2 monolayer in the H_2O and H_3O^+ solvent. HER pathways via the (a) Volmer reaction, (b) Heyrovsky reaction, and (c) Tafel reaction of the La_3C_2 monolayer.

Supporting Tables

Table S1. Structural information of the predicted La_xC_y (x = 2-3, y = 2-3) monolayers.

Phase	Space Group	Lattice Parameters (Å, °)	Wyckoff Positions	Fractional Coordinates		
				x	*y*	*z*
La_2C	*P*-3*m*1	*a* = 3.59130	La(2d)	0.33333	0.66667	0.56982
		b = 3.59130	C(1b)	0.00000	0.00000	0.50000
		c = 20.85170				
		α = 90.0000				
		β = 90.0000				
		γ = 120.0000				
La_3C_2	*P*-3*m*1	*a* = 3.63580	La_1(1b)	0.00000	0.00000	0.50000
		b = 3.63580	La_2(2d)	0.33333	0.66667	0.60091
		c = 29.67060	C(2d)	0.33333	0.66667	0.44078
		α = 90.0000				
		β = 90.0000				
		γ = 120.0000				
La_2C_3	*C*2/*m*	*a* = 5.30520	La(4i)	0.86817	-0.00000	0.43675
		b = 5.07490	C_1(4i)	0.31297	-0.00000	0.46378
		c = 25.28520	C_2(2d)	0.50000	-0.00000	0.50000
		α = 90.0000				
		β = 89.2051				
		γ = 90.0000				
LaC_2	*Pmmn*	*a* = 6.17010	La(2a)	0.50000	0.50000	0.48024
		b = 4.01830	C(4f)	0.60466	0.00000	0.55240
		c = 21.54000				
		α = 90.0000				
		β = 90.0000				
		γ = 90.0000				

Table S2. Cohesive energy (E_{coh}) of the predicted La_xC_y (x = 2-3, y = 2-3) monolayers.

La-C monolayer	E_{coh} (eV)
La_2C	7.39
La_3C_2	7.65
La_2C_3	7.44
LaC_2	7.07

Table S3. Mulliken charge (|e|) analysis of the La_xC_y (x = 2-3, y = 2-3) monolayers.

Atom	La_2C		La_3C_2		La_2C_3		LaC_2	
	Charge (|e|)	ΔG_{H*} (eV)	Charge (|e|)	ΔG_{H*} (eV)	Charge (|e|)	ΔG_{H*} (eV)	Charge (|e|)	ΔG_{H*} (eV)
La_1	0.79	0.58 -0.34 0.19	0.64	-0.09	1.84	2.52	2.12	2.44
La_2	-		-1.35	0.60	-	-	-	
C_1	-1.58	-0.45	-1.67	-0.24	-1.37	0.34	-1.06	0.20 0.13
C_2	-		-	B(La_1-C) 0.03	-0.94	B(C_1-C_2) -0.02 H -0.06	-	 H 0.93

Table S4. Calculated d-ΔG_{H*} and a-ΔG_{H*} (eV) varying different H atoms (n) adsorbed on the La_xC_y (x = 2-3, y = 2-3) monolayers.

n	La_2C		La_3C_2				La_2C_3				LaC_2	
site	H		T_{La1}		B		B		H		T_{C2}	
1	0.19	0.19	-0.09	-0.09	0.03	0.03	-0.02	-0.02	-0.06	-0.06	0.13	0.13
2	0.10	0.15	-0.13	-0.11	~0.0	0.01	-0.04	-0.03	-0.001	-0.03	0.005	0.07
3	~0.0	0.10	-0.02	-0.08	0.03	0.02	-0.11	-0.06	-0.15	-0.07	0.07	0.07
4	0.13	0.10	0.04	-0.05	0.09	0.04	-0.03	-0.05	-0.006	-0.05	0.28	0.12
5	-0.48	-0.01	0.06	-0.03	0.10	0.05	-0.01	-0.04	-0.09	-0.06	0.34	0.16
6	-0.56	-0.10	-0.03	-0.03	0.11	0.06	0.01	-0.03	0.03	-0.05	0.12	0.17
7	0.04	-0.08	0.01	-0.02	0.14	0.07	0.28	0.01			0.42	0.20
8	-1.88	-0.31	-0.05	-0.02	0.17	0.08	0.55	0.08			0.35	0.22
9	2.84	0.04	0.02	-0.02	0.22	0.10					0.69	0.27
10					0.54	0.14						

Table S5. Structural information of the predicted La_xC_y (x = 2-3, y = 2-3) monolayers with increasing H coverage.

Phase	Lattice Parameters (Å, °)	Wyckoff Positions	Fractional Coordinates		
			x	*y*	*z*
La_2C	*a* = 10.80210	La1	0.10823	0.21708	0.53736
	b = 10.80210	La2	0.22200	0.11086	0.46361
	c = 39.53650	La3	0.44051	0.21473	0.53772
	α = 90.0000	La4	0.55544	0.11084	0.46361
	β = 90.0000	La5	0.77512	0.21709	0.53736
	γ = 120.0000	La6	0.88873	0.11085	0.46360
		La7	0.10826	0.55024	0.53712
		La8	0.22205	0.44416	0.46360
		La9	0.44054	0.55144	0.53768
		La10	0.55524	0.44388	0.46451
		La11	0.77718	0.55145	0.53768
		La12	0.88871	0.44415	0.46359
		La13	0.10813	0.88391	0.53711
		La14	0.22207	0.77756	0.46354
		La15	0.44206	0.88391	0.53711
		La16	0.55540	0.77741	0.46358
		La17	0.77504	0.88380	0.53733
		La18	0.88860	0.77742	0.46358
		C1	0.99812	0.99770	0.50028
		C2	0.33175	0.99705	0.49980
		C3	0.66605	0.99772	0.50028
		C4	0.99825	0.33006	0.50032
		C5	0.32220	0.325789	0.49937
		C6	0.67000	0.32582	0.49936
		C7	0.99872	0.66413	0.49979
		C8	0.33185	0.66414	0.49980
		C9	0.67002	0.67360	0.49935
		H1	0.55325	0.44024	0.52224
		H2	0.22279	0.77592	0.52224
		H3	0.88686	0.11032	0.52224
		H4	0.22156	0.44024	0.52224
		H5	0.88800	0.77411	0.52224
		H6	0.55342	0.77257	0.52224

		H7	0.88809	0.44196	0.52224
		H8	0.55727	0.10816	0.52224
		H9	0.22207	0.11039	0.52224

Phase	Lattice Parameters (Å, °)	Wyckoff Positions	Fractional Coordinates		
			x	*y*	*z*
La_3C_2	*a* = 10.91350	La1	0.00015	0.00022	0.49967
	b = 10.91350	La2	0.11242	0.22283	0.57430
	c = 40.32710	La3	0.22218	0.11109	0.42538
	α = 90.0000	La4	0.33346	0.00022	0.49967
	β = 90.0000	La5	0.44392	0.22285	0.57430
	γ = 120.0000	La6	0.55543	0.11119	0.42538
		La7	0.66669	0.00000	0.49952
		La8	0.77744	0.22138	0.57355
		La9	0.88903	0.11119	0.42538
		La10	0.00015	0.33324	0.49967
		La11	0.11101	0.55575	0.57377
		La12	0.22218	0.44444	0.42538
		La13	0.33336	0.33333	0.49964
		La14	0.44393	0.55433	0.57430
		La15	0.55552	0.44444	0.42538
		La16	0.66648	0.33324	0.49967
		La17	0.77826	0.55576	0.57377
		La18	0.88892	0.44458	0.42532
		La19	0.00003	0.66667	0.49956
		La20	0.11101	0.88851	0.57377
		La21	0.22204	0.77770	0.42532
		La22	0.33345	0.66654	0.49967
		La23	0.44541	0.88934	0.57355
		La24	0.55543	0.77759	0.42539
		La25	0.66648	0.66654	0.49967
		La26	0.77744	0.88933	0.57354
		La27	0.88892	0.77770	0.42532
		C1	0.11114	0.22224	0.45602
		C2	0.22166	0.10985	0.54319
		C3	0.44442	0.22224	0.45602
		C4	0.55839	0.10835	0.54274
		C5	0.77854	0.22378	0.45579
		C6	0.88335	0.10833	0.54274
		C7	0.11135	0.55529	0.45601
		C8	0.22166	0.44508	0.54319

	C9	0.44442	0.55551	0.45602
	C10	0.55689	0.44508	0.54319
	C11	0.77726	0.55530	0.45601
	C12	0.88970	0.44594	0.54290
	C13	0.11135	0.88939	0.45601
	C14	0.22080	0.77704	0.54290
	C15	0.44287	0.88810	0.45579
	C16	0.55840	0.78335	0.54274
	C17	0.77855	0.88810	0.45579
	C18	0.88970	0.77704	0.54290
Site T_{La1}	H1	0.33327	0.33335	0.61492
	H2	0.66575	0.33335	0.61492
	H3	0.99931	0.33335	0.61492
	H4	0.66753	0.66885	0.61492
	H5	0.33558	0.00171	0.61492
	H6	0.33455	0.66885	0.61492
	H7	0.00007	0.66770	0.61492
	H8	0.66654	0.00038	0.61492
	H9	0.00137	0.00195	0.61492
Site *B*	H1	0.28276	0.23209	0.54709
	H2	0.95440	0.56598	0.54709
	H3	0.61764	0.89936	0.54709
	H4	0.61567	0.23209	0.54709
	H5	0.27924	0.55974	0.54709
	H6	0.95270	0.23209	0.54709
	H7	0.28214	0.90316	0.54709
	H8	0.61569	0.55961	0.54709
	H9	0.94723	0.90108	0.54709

Phase	Lattice Parameters (Å, °)	Wyckoff Positions	Fractional Coordinates		
			x	*y*	*z*
La_2C_3	*a* = 10.61520	La1	0.43268	0.99709	0.45915
	b = 10.10080	La2	0.18342	0.24757	0.45984
	c = 39.68460	La3	0.07103	0.00689	0.54019
	α = 90.0000	La4	0.31879	0.26232	0.54172
	β = 89.2051	La5	0.93361	0.99707	0.45943
	γ = 90.0000	La6	0.68237	0.24581	0.45979
		La7	0.56831	0.00700	0.54043
		La8	0.81947	0.25803	0.54033
		La9	0.43705	0.49675	0.45622
		La10	0.18355	0.74674	0.46000

	La11	0.07296	0.50686	0.54040
	La12	0.31899	0.75191	0.54187
	La13	0.92900	0.49717	0.45950
	La14	0.68250	0.74852	0.45993
	La15	0.56554	0.50661	0.53883
	La16	0.81949	0.75596	0.54051
	C1	0.15641	0.99929	0.47707
	C2	0.90655	0.24850	0.47689
	C3	0.34508	0.00436	0.52360
	C4	0.09723	0.25578	0.52302
	C5	0.25195	0.00176	0.50004
	C6	0.00130	0.25162	0.50007
	C7	0.65561	0.99928	0.47705
	C8	0.40716	0.24908	0.47653
	C9	0.84607	0.00489	0.52315
	C10	0.59511	0.25392	0.52327
	C11	0.75133	0.00205	0.50002
	C12	0.49994	0.25127	0.50016
	C13	0.15323	0.49886	0.47417
	C14	0.90685	0.75005	0.47705
	C15	0.34950	0.50460	0.51755
	C16	0.09759	0.75389	0.52318
	C17	0.25062	0.50174	0.49650
	C18	0.00151	0.75263	0.50026
	C19	0.65499	0.49929	0.47700
	C20	0.40753	0.74931	0.47658
	C21	0.84821	0.50490	0.52275
	C22	0.59517	0.75589	0.52340
	C23	0.75003	0.50213	0.50035
	C24	0.50006	0.75296	0.50027
	H1	0.28441	0.50343	0.57831
	H2	0.27204	0.99620	0.57949
	H3	0.05807	0.25291	0.58012
	H4	0.54091	0.24894	0.57954
	H5	0.06547	0.74892	0.58029
	H6	0.54091	0.74566	0.57963
	H7	0.80850	0.49964	0.58244
	H8	0.81801	0.00443	0.58246
Site *H*	H1	0.45299	0.35560	0.58163
	H2	0.45928	0.64530	0.58185
	H3	0.92993	0.61390	0.58044
	H4	0.70477	0.62951	0.58112
	H5	0.17229	0.35518	0.58245
	H6	0.68501	0.35304	0.58094

Phase	Lattice Parameters (Å, °)	Wyckoff Positions	Fractional Coordinates		
			x	*y*	*z*
LaC_2	*a* = 12.30500	La1	0.24928	0.16802	0.48563
	b = 12.17860	La2	0.99307	0.00004	0.50682
	c = 37.00550	La3	0.74808	0.16699	0.48793
	α = 90.0000	La4	0.49158	0.00004	0.50934
	β = 90.0000	La5	0.24946	0.50003	0.50031
	γ = 90.0000	La6	0.99219	0.32516	0.51297
		La7	0.75036	0.50001	0.48973
		La8	0.49155	0.33709	0.51358
		La9	0.24928	0.83201	0.48563
		La10	0.99219	0.67494	0.51297
		La11	0.74808	0.83303	0.48793
		La12	0.49155	0.66300	0.51358
		C1	0.28907	0.00006	0.52498
		C2	0.18386	0.00006	0.52448
		C3	0.95102	0.16963	0.46653
		C4	0.05594	0.16873	0.46584
		C5	0.79030	0.00006	0.52948
		C6	0.68546	0.00006	0.52956
		C7	0.45303	0.17066	0.46901
		C8	0.55762	0.16861	0.46885
		C9	0.28743	0.31312	0.53448
		C10	0.18319	0.31744	0.53505
		C11	0.95538	0.50000	0.47743
		C12	0.06088	0.50000	0.47818
		C13	0.79069	0.32957	0.52994
		C14	0.68571	0.33389	0.52994
		C15	0.44809	0.50000	0.46690
		C16	0.55209	0.49999	0.46667
		C17	0.28743	0.68703	0.53448
		C18	0.18319	0.68270	0.53505
		C19	0.95102	0.83036	0.46653
		C20	0.05594	0.83126	0.46584
		C21	0.79069	0.67055	0.52994
		C22	0.68571	0.66623	0.52994
		C23	0.45303	0.82934	0.46901

C24	0.55762	0.83138	0.46885
H1	0.41122	0.50008	0.53930
H2	0.58337	0.16616	0.53391
H3	0.09689	0.50015	0.54588
H4	0.07816	0.83270	0.53592
H5	0.56866	0.49789	0.53441
H6	0.43888	0.83202	0.53849
H7	0.43681	0.16853	0.53846
H8	0.59343	0.83736	0.53369

References

1 Y. Wang, J. Lv, L. Zhu and Y. Ma, *Comput. Phys. Commun.*, 2012, **183**, 2063–2070.

2 Y. Wang, J. Lv, L. Zhu and Y. Ma, *Phys. Rev. B.*, 2010, **82**, 094116.

3 G. Kresse and J. Furthmüller, *Phys. Rev. B*, 1996, **54**, 11169–11186.

4 J. Y. Jung, J. H. Park, Y. J. Jeong, K. H. Yang, N. K. Choi, S. H. Kim and W. J. Kim, *Phys. Rev.*, 1965, **140**, A1133–A1138.

5 J. P. Perdew, K. Burke and M. Ernzerhof, *Phys. Rev. Lett.*, 1996, **77**, 3865–3868.

6 G. J. Martyna, M. L. Klein and M. Tuckerman, *J. Chem. Phys.*, 1992, **97**, 2635–2643.

7 S. Haastrup, M. Strange, M. Pandey, T. Deilmann, P. S. Schmidt, N. F. Hinsche, M. N. Gjerding, D. Torelli, P. M. Larsen, A. C. Riis-Jensen, J. Gath, K. W. Jacobsen, J. J. Mortensen, T. Olsen and K. S. Thygesen, *2D Mater.*, 2019, 048001.